

Metastable Carbon at Extreme Conditions

Ashley S. Williams, Kien Nguyen-Cong, Jonathan T. Willman, and Ivan I. Oleynik*
Department of Physics, University of South Florida, Tampa, FL 33620

Carbon at extreme conditions is the focus of intensive scientific inquiry due to its importance for applications in inertial confinement fusion experiments and for understanding the interior structure of carbon-rich exoplanets. The extreme metastability of diamond at very high pressures has been discovered in recent dynamic compression experiments. This work addresses an important question about the existence of other competitive metastable carbon phases that might be observed in shock experiments. It was found that diamond polytypes, carbon crystals with mixed cubic and hexagonal diamond stacking planes, are the only metastable carbon crystal phases energetically competitive with cubic diamond at pressures between 100 and 1,000 GPa. Above 1 TPa, no metastable phases are found to be energetically competitive with thermodynamically stable BC8 and simple cubic phases. The existence of low enthalpy diamond polytypes suggests that they are likely candidates for metastable phases of carbon to appear upon shockwave loading of diamond.

Carbon, one of the most frequently occurring elements in the universe, is unique due to its ability to form sp , sp^2 , and sp^3 hybrid orbitals resulting in numerous metastable allotropes at ambient conditions in addition to thermodynamically stable graphite and slightly metastable cubic diamond (CD). Although carbon is well studied at ambient conditions its behavior at extreme conditions is not well understood. Recently, the high pressure behavior of carbon has attracted substantial effort, both experimentally [1–13] and theoretically [14–25].

Not much is known about the metastability of carbon under extreme conditions and the topic has become somewhat controversial as new experimental and simulation methods become prevalent. For instance, while Knudson *et al.*[3] showed the appearance of BC8 phase near the triple point, recent dynamic compression at NIF[7] failed to observe transition of CD to BC8 and instead suggested a high energy barrier between the two phases. The notion of a high energy barrier lead to the proposal of metastability of diamond extending well beyond its region of thermodynamic stability, which begs the question- are there metastable phases at extreme conditions that are being missed with conventional methods? Along the same line, x-ray diffraction experiments have claimed to observe hexagonal diamond from shock loading of both graphite [11–13, 26] and diamond [8, 27–29], however, there are still questions surrounding these observations. One major question being posed is whether or not it is possible to resolve such smaller differences in the crystals and definitively say when transformation had occurred. This work aims to answer these questions with a systematic study of carbon up to 5 TPa under uniaxial shock compression conditions as this is the only way to experimentally reach such high pressures in carbon. We find that carbon forms few energetically competitive metastable structures at high pressures other than the known thermodynamically stable phases of graphite, CD, BC8, and simple cubic (SC). Diamond polytypes, a class of carbon

crystal that contains mixing of CD stacking and hexagonal diamond (HD) stacking, were the only competitive phases possible in pressures up to 1 TPa. In agreement with previous investigations [14, 19], there were no phases found that could compete with thermodynamically stable BC8 or SC above 1TPa.

In order to simulate shock wave conditions, we extend the crystal structure prediction method [30–32] beyond hydrostatic conditions by applying uniaxial compression to the unit cell of diamond. The evolutionary algorithm in the crystal structure prediction method works by ranking individuals via enthalpy which is not uniquely defined under uniaxial compression. Therefore, careful consideration of the energetics of predicted crystals that mimics shock wave experiments must take place. First, rapid uniaxial compression takes places via the search followed by relaxation to hydrostatic conditions at a given pressure then final release to ambient conditions. All individuals from the final generation of the search are considered in order to get accurate rankings upon the two instances of hydrostatic relaxation. The protocol is detailed in Fig. 1.

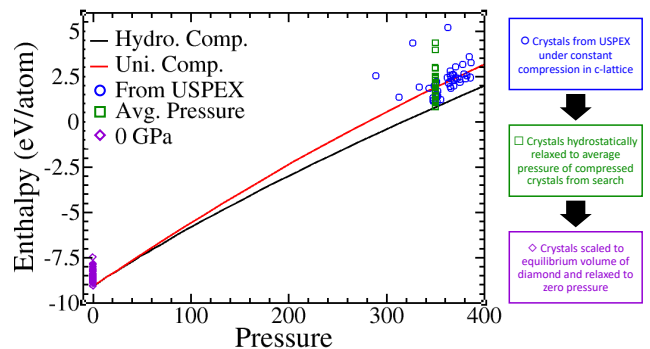


Figure 1. Schematic showing procedure for analysis of uniaxially compressed USPEX searches. Black line corresponds to the hydrostatic compression of diamond. Red line corresponds to uniaxial compression of $\langle 100 \rangle$ diamond. Structures originated from search at fixed lattice corresponding to $\langle 100 \rangle$ diamond with longitudinal stress of 500 GPa.

* oleynik@usf.edu

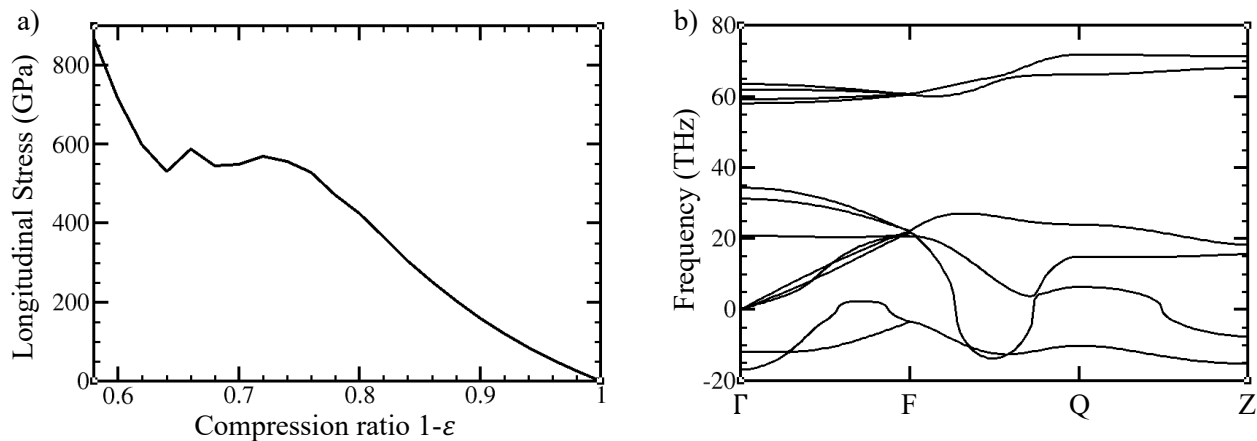


Figure 2. a) Stress versus strain curve for uniaxially compressed $\langle 110 \rangle$ diamond with change in slope around 500 GPa suggesting instability of the crystal beyond this point. b) Calculated phonon spectra of $\langle 110 \rangle$ diamond uniaxially compressed to 500 GPa longitudinal stress with negative frequencies.

We used this protocol to confirm the previously known hydrostatic phase diagram of carbon [19, 20] up to 5 TPa via several first-principles crystal structure searches at pressures ranging from 100 to 5000 GPa. All predicted crystals within 0.1 eV/atom of the lowest enthalpy crystal from the final generation of the search were considered for the hydrostatic phase diagram. While the story of hydrostatically compressed carbon is a simple one to theoretically explore and tell, its behavior under uniaxial compression is not. Investigation of the stress-strain curve of uniaxially compressed $\langle 110 \rangle$ diamond shows non-monotonic behavior suggesting instability in the crystal, see Fig. 2a. Phonon band structure of the $\langle 110 \rangle$ diamond uniaxially compressed to 500 GPa longitudinal stress, Fig. 2b, shows negative frequencies indicating there is indeed dynamic instability of the crystal under uniaxial compression. Searches at 100 GPa longitudinal stress predict conventional uniaxially compressed diamond to be the preferred orientation. However, we predict rearrangement of the atoms inside the unit cell for most searches performed under uniaxial compression at longitudinal stresses greater than 100 GPa. The searches predict that diamond polytypes, i.e. crystals that contain a mixture of CD and HD stacking, are the most likely metastable phases able to be achieved during shock experiments up to 1 TPa. These results suggest that shock compression of diamond beyond 100 GPa longitudinal stress is necessary to observe a transformation into these predicted phases. Despite the suggestion[28] that HD is formed via shock compression of diamond, our results predict that diamond polytype crystals with lower hexagonality are energetically preferred as seen in Figure 3. Here we define the hexagonality of a crystal as the ratio of the number of HD layers to the total number of layers; with a layer being defined as two consecutive atoms in the same c-lattice plane. For naming convention, we will refer to all polytypes by their symmetry and number of layers. As a rise in temperature is inherently associated

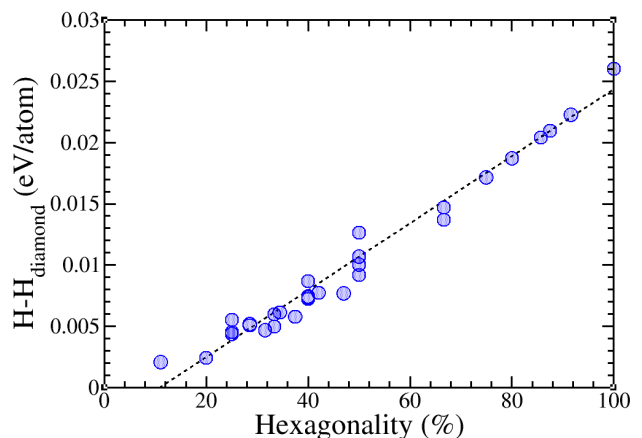


Figure 3. Relative enthalpy of a sample of diamond polytypes as a function of hexagonality showing an increasing trend from fully CD stacked crystal to fully HD stacked crystal. Crystal structure for polytypes not found in our searches or built by hand taken from databases [33, 34].

with shock compression, we provide the temperature dependence of the enthalpies of a sample of polytypes along with HD in Figure S6.

Four diamond polytypes and HD are predicted across our searches. Two polytypes, $P6_3/mmc-4$ and $R3m-12$, have 50% hexagonality while the other two polytypes, $R3m-9$ and $R3m-18$, have 66.7% hexagonality. Snapshots of the predicted polytypes can be seen in Fig. 4a. Beyond the diamond polytypes, three 3D mesh structures are predicted to be in the metastable region at low pressures. Snapshots of these crystals are displayed in Figure S7. The enthalpies of these crystals are much higher than the diamond polytypes so their appearance under shock compression is unlikely. Mujica *et al.* predicted a crystal with symmetry $Pbam$ that had a similar 5/6/7 membered ring network to what is seen in Figure S7a-b

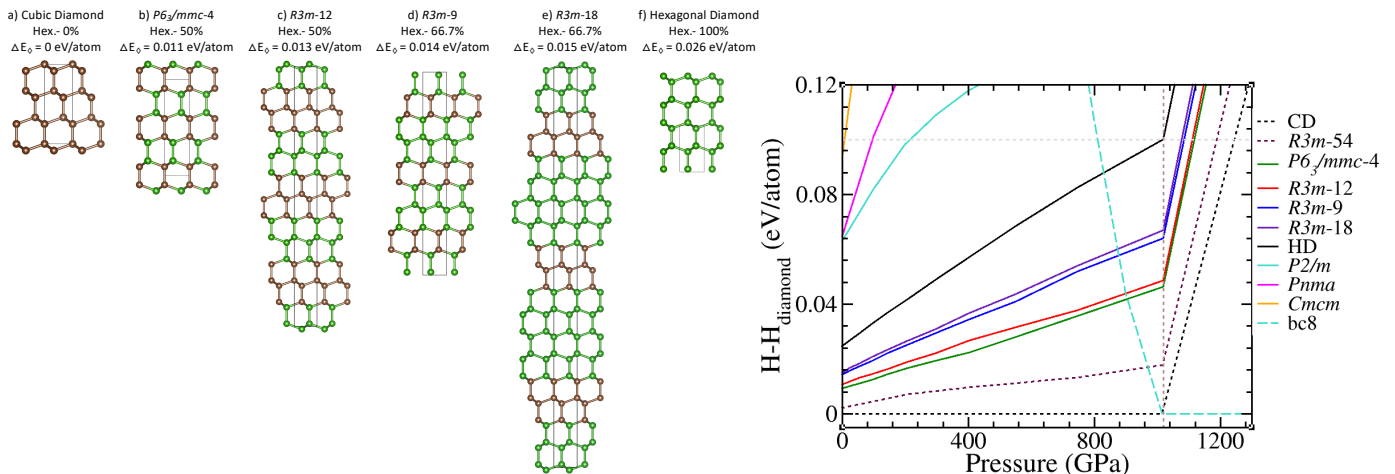


Figure 4. a) Snapshots of polytypes predicted in first-principles searches; brown atoms denote CD stacking and green atoms denote HD stacking. b) Energetics of predicted metastable crystals found across all searches. The maroon dashed line corresponds to the lowest enthalpy diamond polytype samples from databases. Reference structure to the left of the brown vertical dashed line is CD, while BC8 is used as the reference to the right.

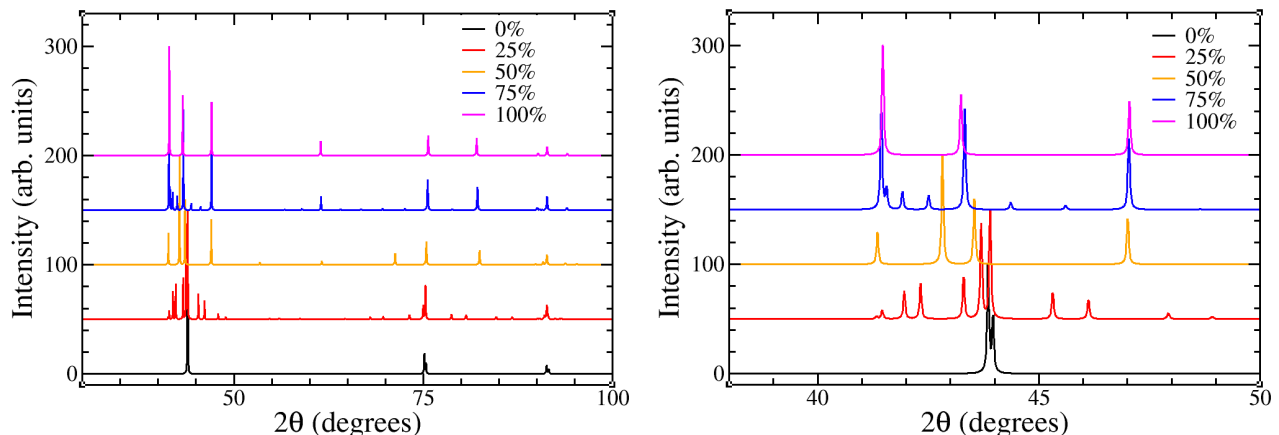


Figure 5. XRD patterns of diamond polytypes.

and also predicted the existence of a new chiral framework with tetragonal symmetry $P4_12_12$. We observe this $P4_12_12$ crystal in our searches as well, however it does not meet our enthalpy requirement for metastability.

Past experiments have claimed to observe hexagonal diamond from shock loading both graphite [11–13, 25, 26] and diamond [28], however, there are still questions surrounding these observations. One major question being posed is whether or not it is possible to resolve such small differences in the crystals and definitively say what transformation has occurred. X-ray diffraction (XRD) patterns for several mixtures of cubic and hexagonal diamond polytypes (Figure 5) suggest that the differences in the crystal lattice of various polytypes can indeed be resolved. In fact, a clear trend can be observed in the XRD as the polytypes increase in hexagonality. The peak in CD at 44 degrees can be seen to split as the hexagonality of the crystal grows. In polytypes with hexagonality greater than 50%, there are clear peaks that grow at

62 and 82 degrees. Recently, it has been proposed that diamond-graphene composite structures will appear under shock wave loading instead of the diamond polytypes presented here and while HRTEM images do appear to show areas of the composite structure in impact diamonds confirmation of these findings via XRD patterns is not conclusive [9, 10]. Nemeth *et al.* state that the areas of these composite structures are small [9], which make capturing them by XRD challenging. While some composite structures do have a comparable enthalpy difference to diamond polytypes at very low pressures, the same cannot be said for these structures at even moderate pressure (see Figure S9). This is consistent with the behavior of graphene, which becomes less favorable to diamond very rapidly at low pressures. These factors, combined with the trend we observe in our simulated x-ray diffraction patterns of diamond polytypes as they grow in hexagonality, lead to the conclusion that the appearance of the composite structures in the HRTEM images

are the result of anisotropic conditions in the impact diamond. The class of diamond polytypes detailed in this work should still be considered the leading candidates for controlled shock experiments on diamond.

In conclusion, a unique method of crystal structure prediction has been employed to explore the effect of shock wave loading on a fixed unit cell. The previously known hydrostatic phase diagram of carbon is confirmed via both the new method and the traditional fixed pressure crystal structure searches. The new method also predicts diamond polytypes of mixed cubic diamond and hexagonal diamond stacking to be energetically preferred to conventional uniaxially compressed diamond at longitudinal stresses exceeding 100 GPa. The existence of these low enthalpy polytypes suggests that they are the likely candidates for metastable phases of carbon to appear upon shockwave loading of diamond. It is therefore unlikely that recently proposed complex crystalline forms [9, 23, 24] would result from shock experiments. Finally, calculated XRD patterns show that the resolution of diamond polytypes that result from the shock compression of diamond should be distinguishable from both cubic diamond and hexagonal diamond.

METHODS

We performed several crystal structure searches using USPEX [30–32], an evolutionary algorithm that works

in generations, to predict the most energetically favorable crystal for a given environment. The enthalpy of the crystals in each generation is minimized using the density functional theory (DFT) code VASP[35] by relaxing the unit cell parameters and atomic positions for a fixed hydrostatic pressure. At the end of each generation, the crystals are ranked according to their enthalpy with the lowest enthalpy individual being the best candidate for that generation. This cyclic process repeats until the best individual is kept for ten generations. To investigate the hydrostatic phase diagram of carbon, searches were performed at fixed pressures of 100, 500, 1000, 3000, and 5000 GPa. To mimic the environment of shock-compressed diamond, searches were performed for crystals with fixed lattice vectors corresponding to 100, 300, 500, and 1000 GPa longitudinal stress for $\langle 100 \rangle$, $\langle 110 \rangle$, and $\langle 111 \rangle$ diamond. During these searches, only the atoms were relaxed to ensure the uniaxial compression environment was maintained. See supplemental information for full methods details.

-
- [1] K.-I. Kondo and T. J. Ahrens, *Geophys. Res. Lett.* **10**, 281 (1983).
- [2] S. Scandolo, M. Bernasconi, G. L. Chiarotti, P. Focher, and E. Tosatti, *Phys. Rev. Lett.* **74**, 4015 (1995).
- [3] M. D. Knudson, M. P. Desjarlais, and D. H. Dolan, *Science* **322**, 1822 (2008).
- [4] J. H. Eggert, D. G. Hicks, P. M. Celliers, D. K. Bradley, R. S. McWilliams, R. Jeanloz, J. E. Miller, T. R. Boehly, and G. W. Collins, *Nat. Phys.* **6**, 40 (2010).
- [5] R. S. McWilliams, J. H. Eggert, D. G. Hicks, D. K. Bradley, P. M. Celliers, D. K. Spaulding, T. R. Boehly, G. W. Collins, and R. Jeanloz, *Phys. Rev. B* **81**, 014111 (2010).
- [6] D. Kraus, A. Otten, A. Frank, V. Bagnoud, A. Blažević, D. Gericke, G. Gregori, A. Ortner, G. Schaumann, D. Schumacher, J. Vorberger, F. Wagner, K. Wünsch, and M. Roth, *High Energy Density Phys.* **8**, 46 (2012).
- [7] R. F. Smith, J. H. Eggert, R. Jeanloz, T. S. Duffy, D. G. Braun, J. R. Patterson, R. E. Rudd, J. Biener, A. E. Lazicki, A. V. Hamza, J. Wang, T. Braun, L. X. Benedict, P. M. Celliers, and G. W. Collins, *Nature* **511**, 330 (2014).
- [8] A. P. Jones, P. F. McMillan, C. G. Salzmann, M. Alvaro, F. Nestola, M. Prencipe, D. Dobson, R. Hazael, and M. Moore, *Lithos* **265**, 214 (2016).
- [9] P. Németh, K. McColl, R. L. Smith, M. Murri, L. A. J. Garvie, M. Alvaro, B. Pécz, A. P. Jones, F. Corà, C. G. Salzmann, and P. F. McMillan, *Nano Lett.* **20**, 3611 (2020).
- [10] P. Németh, K. McColl, L. A. J. Garvie, C. G. Salzmann, M. Murri, and P. F. McMillan, *Nat. Mater.* **19**, 1126 (2020).
- [11] S. J. Turneaure, S. M. Sharma, T. J. Volz, J. M. Winey, and Y. M. Gupta, *Sci. Adv.* **3**, eaao3561 (2017).
- [12] E. Stavrou, M. Bagge-Hansen, J. A. Hammons, M. H. Nielsen, B. A. Steele, P. Xiao, M. P. Kroonblawd, M. D. Nelms, W. L. Shaw, W. Bassett, S. Bastea, L. M. Lauderbach, R. L. Hodgkin, N. A. Perez-Marty, S. Singh, P. Das, Y. Li, A. Schuman, N. Sinclair, K. Fezzaa, A. Deriy, L. D. Leininger, and T. M. Willey, *Phys. Rev. B* **102**, 104116 (2020).
- [13] T. J. Volz, S. J. Turneaure, S. M. Sharma, and Y. M. Gupta, *Phys. Rev. B* **101**, 224109 (2020).
- [14] A. A. Correa, L. X. Benedict, D. A. Young, E. Schwegler, and S. A. Bonev, *Phys. Rev. B* **78**, 024101 (2008).
- [15] I. I. Oleynik, A. C. Landerville, S. V. Zybin, M. L. Elert, and C. T. White, *Phys. Rev. B* **78**, 180101 (2008).
- [16] B. Wen, J. Zhao, M. J. Bucknum, P. Yao, and T. Li, *Diam. Relat. Mater.* **17**, 356 (2008).
- [17] J. Sun, D. D. Klug, and R. Martoňák, *J. Chem. Phys.* **130**, 194512 (2009).
- [18] Q. Zhu, A. R. Oganov, M. A. Salvadó, P. Perterra, and A. O. Lyakhov, *Phys. Rev. B* **83**, 193410 (2011).

- [19] M. Martinez-Canales, C. J. Pickard, and R. J. Needs, Phys. Rev. Lett. **108**, 045704 (2012).
- [20] A. R. Oganov, R. J. Hemley, R. M. Hazen, and A. P. Jones, Rev. Mineral. Geochemistry **75**, 47 (2013).
- [21] N. Pineau, J. Phys. Chem. C **117**, 12778 (2013).
- [22] H.-J. Cui, X.-L. Sheng, Q.-B. Yan, Z.-G. Zhu, Q.-R. Zheng, and G. Su, Comput. Mater. Sci. **98**, 129 (2015).
- [23] A. Mujica, C. J. Pickard, and R. J. Needs, Phys. Rev. B **91**, 214104 (2015), arXiv:1508.02631.
- [24] Z.-Z. Li, J.-T. Wang, H. Mizuseki, and C. Chen, Phys. Rev. B **98**, 094107 (2018).
- [25] S. Zhu, X. Yan, J. Liu, A. Oganov, and Q. Zhu, SSRN Electron. J. , 1 (2020).
- [26] J. Dong, Z. Yao, M. Yao, R. Li, K. Hu, L. Zhu, Y. Wang, H. Sun, B. Sundqvist, K. Yang, and B. Liu, Phys. Rev. Lett. **124**, 65701 (2020).
- [27] W. Baek, S. A. Gromilov, A. V. Kuklin, E. A. Kovaleva, A. S. Fedorov, A. S. Sukhikh, M. Hanfland, V. A. Pomogaev, I. A. Melchakova, P. V. Avramov, and K. V. Yusenko, Nano Lett. **19**, 1570 (2019).
- [28] H. He, T. Sekine, and T. Kobayashi, Appl. Phys. Lett. **81**, 610 (2002).
- [29] M. Murri, R. L. Smith, K. McColl, M. Hart, M. Alvaro, A. P. Jones, P. Németh, C. G. Salzmann, F. Corà, M. C. Domeneghetti, F. Nestola, N. V. Sobolev, S. A. Vishnevsky, A. M. Logvinova, and P. F. McMillan, Sci. Rep. **9**, 10334 (2019).
- [30] C. W. Glass, A. R. Oganov, and N. Hansen, Comput. Phys. Commun. **175**, 713 (2006).
- [31] A. R. Oganov and C. W. Glass, J. Chem. Phys. **124**, 244704 (2006).
- [32] A. O. Lyakhov, A. R. Oganov, and M. Valle, Comput. Phys. Commun. **181**, 1623 (2010).
- [33] A. Jain, S. P. Ong, G. Hautier, W. Chen, W. D. Richards, S. Dacek, S. Cholia, D. Gunter, D. Skinner, G. Ceder, and K. A. Persson, APL Mater. **1**, 011002 (2013).
- [34] S. Gražulis, D. Chateigner, R. T. Downs, A. F. T. Yokochi, M. Quirós, L. Lutterotti, E. Manakova, J. Butkus, P. Moeck, and A. Le Bail, J. Appl. Crystallogr. **42**, 726 (2009).

- [35] G. Kresse and J. Furthmüller, Phys. Rev. B **54**, 11169 (1996).

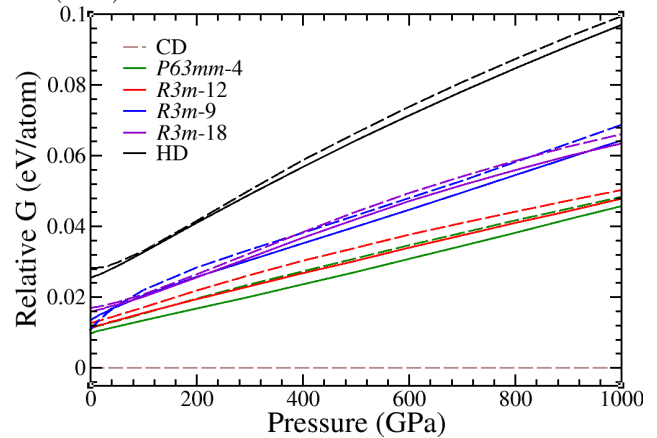


Figure 6. Temperature dependence of enthalpy for selected polytypes showing no significant changes.

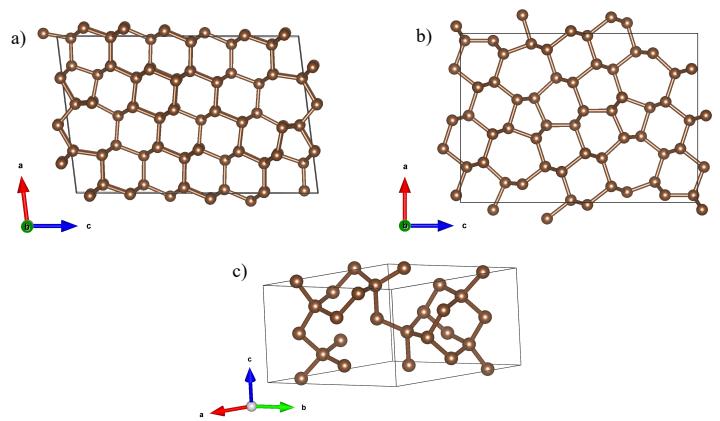


Figure 7.

SUPPLEMENTAL FIGURES

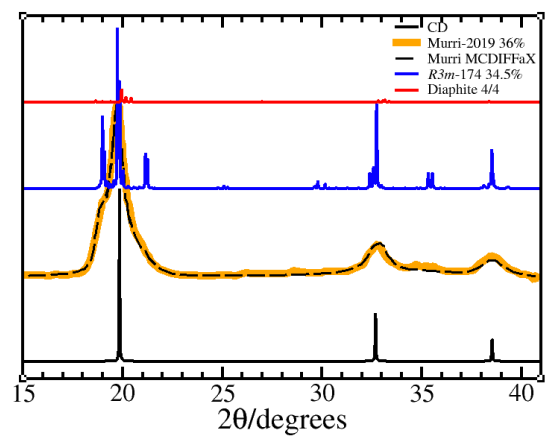


Figure 8.

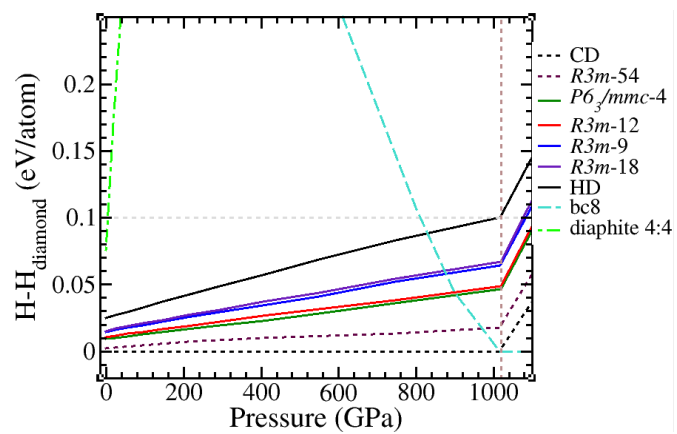


Figure 9.